Fractional Calculus & Applied Analysis
An International Journal for Theory and Applications
VOLUME 11, NUMBER 1 (2008) ISSN 1311-0454

APPLICATION OF FRACTIONAL CALCULUS IN THE DYNAMICAL ANALYSIS AND CONTROL OF MECHANICAL MANIPULATORS

N. M. Fonseca Ferreira [1], Fernando B. Duarte [2], Miguel F. M. Lima [3], Maria G. Marcos [4], J. A. Tenreiro Machado [5]

Abstract

Fractional Calculus (FC) goes back to the beginning of the theory of differential calculus. Nevertheless, the application of FC just emerged in the last two decades. In the field of dynamical systems theory some work has been carried out but the proposed models and algorithms are still in a preliminary stage of establishment. This article illustrates several applications of fractional calculus in robot manipulator path planning and control.

Mathematics Subject Classification: 26A33, 93C83, 93C85, 68T40
Key Words and Phrases: fractional calculus, robotics, modeling, dynamics

1. Introduction

Fractional calculus (FC) is a natural extension of the classical mathematics but, in spite of the work that has been done recently, the application of FC in the analysis and control of dynamical systems is still reduced. In this line of thoughts this paper addresses the application of FC in the robotic manipulating systems and is organized as follows. Section 2 studies the trajectory planning of redundant manipulators through the adoption of the pseudoinverse of the jacobian and its influence of the fractional dynamics that occurs in the joint variables. Section 3 analyzes the spectra of several signals in industrial manipulators that exhibit vibrations due to a

[5]Corresponding author

non-ideal mechanical structure and to impacts of gripper. Sections 4 and 5 investigate the performance of fractional order algorithms in the position and force control of one arm in contact with a surface and two cooperating arms, respectively. Finally, Section 6 draws the main conclusions.

2. Trajectory control of redundant manipulators

A kinematically redundant manipulator is a robotic arm possessing more degrees of freedom (dof) than those required to establish an arbitrary position and orientation of the gripper. Redundant manipulators offer several potential advantages over non-redundant arms. In a workspace with obstacles, the extra degrees of freedom can be used to move around or between obstacles and thereby to manipulate in situations that otherwise would be inaccessible, see [1]–[4]. When a manipulator is redundant, it is anticipated that the inverse kinematics admits an infinite number of solutions. This implies that, for a given location of the manipulator's gripper, it is possible to induce a self-motion of the structure without changing the location of the end effecter. Several kinematic techniques for redundant manipulators control the gripper through the rates at which the joints are driven, using the pseudoinverse of the Jacobian [3], [5]. Nevertheless, these algorithms lead to a kind of chaotic motion with unpredictable arm configurations.

A kinematically redundant manipulator is a robotic arm possessing more dof than those required to establish an arbitrary position and orientation of the gripper. In **Fig. 1** is depicted a planar manipulator with $k \in N$ rotational (R) joints that is redundant for $k > 2$. Therefore, redundant manipulators can be reconfigured to find better postures for an assigned set of task requirements but, on the other hand, have a more complex structure requiring adequate control algorithms.

We consider a manipulator with n degrees of freedom whose joint variables are denoted by $\mathbf{q} = [q_1, q_2, ..., q_n]^T$. We assume that a class of tasks we are interested in can be described by m variables, $\mathbf{x} = [x_1, x_2, ..., x_m]^T$ ($m < n$) and that the relation between $\mathbf{q}$ and $\mathbf{x}$ is given by:

$$\mathbf{x} = \boldsymbol{f}(\mathbf{q}), \tag{1}$$

where f is a function representing the direct kinematics. Differentiating (1) with respect to time yields:

$$\dot{\mathbf{x}} = \mathbf{J}(\mathbf{q})\dot{\mathbf{q}}, \tag{2}$$

where $\dot{\mathbf{x}} \in \Re^m$ and $\mathbf{J}(\mathbf{q}) = \partial f(\mathbf{q})/\partial \mathbf{q} \in \Re^{m \times n}$. Hence, it is possible to calculate a path $\mathbf{q}(t)$ in terms of a prescribed trajectory $\mathbf{x}(t)$ in the operational space. We assume that the following condition is satisfied:

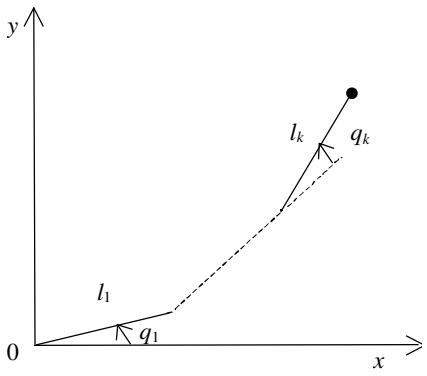

Figure 1: A planar redundant planar manipulator with k rotational joints.

$$max \quad rank\{\mathbf{J(q)}\} = m. \tag{3}$$

Failing to satisfy this condition usually means that the selection of manipulation variables is redundant and the number of these variables m can be reduced. When condition (3) is verified, we say that the degree of redundancy of the manipulator is $n - m$. If, for some $\mathbf{q}$ we have:

$$rank\{\mathbf{J(q)}\} < m, \tag{4}$$

then the manipulator is in a singular state. This state is not desirable because, in this region of the trajectory, the manipulating ability is very limited.

Many approaches for solving redundancy [5]–[7] are based on the inversion of equation (2). A solution in terms of the joint velocities is sought as:

$$\dot{\mathbf{q}} = \mathbf{J}^{\#}(\mathbf{q})\dot{\mathbf{x}}, \tag{5}$$

where $\mathbf{J}^{\#}$ is one of the generalized inverses of the $\mathbf{J}$, see [7]–[9]. It can be easily shown that a more general solution to equation (2) is given by:

$$\dot{\mathbf{q}} = \mathbf{J}^{+}(\mathbf{q})\dot{\mathbf{x}} + [\mathbf{I} - \mathbf{J}^{+}(\mathbf{q})\mathbf{J}(\mathbf{q})]\dot{\mathbf{q}}_0, \tag{6}$$

where $\mathbf{I}$ is the $n \times n$ identity matrix and $\dot{\mathbf{q}}_0$ is a $n \times 1$ arbitrary joint velocity vector and $\mathbf{J}^{+}$ is the pseudoinverse of the $\mathbf{J}$. The solution (6) is composed of two terms. The first term is relative to minimum norm joint velocities. The second term, the homogeneous solution, attempts to satisfy the additional constraints specified by $\dot{\mathbf{q}}_0$. Moreover, the matrix $\mathbf{I} - \mathbf{J}^{+}(\mathbf{q})\mathbf{J}(\mathbf{q})$ allows the projection of $\dot{\mathbf{q}}_0$ in the null space of $\mathbf{J}$. A direct consequence

is that it is possible to generate internal motions that reconfigure the manipulator structure without changing the gripper position and orientation, [7]–[9]. Another aspect revealed by the solution of (5) is that repetitive trajectories in the operational space do not lead to periodic trajectories in the joint space. This is an obstacle for the solution of many tasks because the resultant robot configurations have similarities with those of a chaotic system.

The direct kinematics and the Jacobian of a 3-link planar manipulator with rotational joints ($3R-$robot) has a simple recursive nature according with the expressions:

$$\begin{bmatrix} x \\ y \end{bmatrix} = \begin{bmatrix} l_1 C_1 + l_2 C_{12} + l_3 C_{123} \\ l_1 S_1 + l_2 S_{12} + l_3 S_{123} \end{bmatrix}, \tag{7}$$

$$\mathbf{J} = \begin{bmatrix} -l_1 S_1 - ... - l_3 S_{123} ... - l_3 S_{123} \\ l_1 C_1 + ... + l_3 C_{123} ... + l_3 C_{123} \end{bmatrix}, \tag{8}$$

where l_i is the length of link i, $q_{i..k} = q_i + ... + q_k$, $S_{i..k} = Sin(q_{i..k})$ and $C_{i..k} = Cos(q_{i..k})$. During all the experiments it is considered $\Delta t = 10^{-3}$ sec, $L_{TOT} = l_1 + l_2 + l_3 = 3$ and $l_1 = l_2 = l_3$. In the closed-loop pseudoinverse's method the joint positions can be computed through the time integration of the velocities according with the block diagram of the inverse kinematics algorithm depicted in **Fig. 2** where $\mathbf{x}_{ref}$ represents the vector of reference coordinates of the robot gripper in the operational space. Based on equation (8) we analyze the kinematic performances of the $3R-$robot when repeating a circular motion in the operational space with frequency $\omega_0 = 7.0$ rad sec^{-1}, centre at distance $r = [x^2 + y^2]^{1/2}$ and radius ρ. **Fig. 3** shows the joint positions for the inverse kinematic algorithm (5) for $r = \{0.6, 2.0\}$ and $\rho = \{0.3, 0.5\}$. We observe that:

- For $r = 0.6$ occur unpredictable motions with severe variations that lead to high joint transients [10]. Moreover, we verify a low frequency signal modulation that depends on the circle being executed.
- For $r = 2.0$ the motion is periodic with frequency identical to $\omega_0 = 7.0$ rad sec^{-1}.

Previously, we verified that the pseudoinverse based algorithm leads to unpredictable arm configurations. In order to gain further insight into the pseudoinverse nature several distinct experiments are devised in the sequel during a time window of 300 cycles. Therefore, in a first set of experiments we calculate the Fourier transform of the $3R-$robot joints velocities

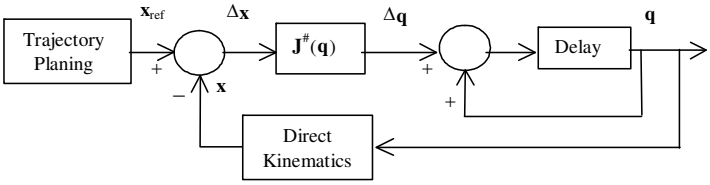

Figure 2: Block diagram of the closed-loop inverse kinematics algorithm with the pseudoinverse.

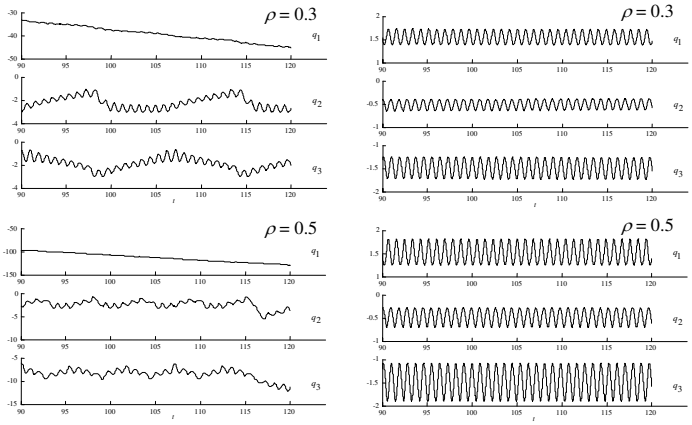

Figure 3: The $3R-$robot joint positions versus time using the pseudoinverse method for $r = \{0.6,\ 2.0\}$ and $\rho = \{0.3,\ 0.5\}$.

for a circular repetitive motion with frequency $\omega_0 = 7.0$ rad sec^{-1}, radius $\rho = \{0.3,\ 0.5\}$ and radial distances $r \in]0,\ L_{TOT}\text{-}\rho[$. **Fig. 4** shows $|F\{\dot{q}_2(t)\}|$ *versus* the frequency ratio ω_0/ω and the distance r, where $F\{\}$ represents the Fourier operator. It is verified an interesting phenomenon induced by the gripper repetitive motion ω_0 because a large part of the energy is distributed along several sub-harmonics. These fractional order harmonics (foh) depend on r and ρ making a complex pattern with similarities with those revealed by chaotic systems. Joints 1 and 3 show similar velocity spectra. In the authors' best knowledge, the foh are aspects of fractional dynamics [11]–[13], but a final and assertive conclusion about a physical

interpretation is a matter still to be explored.

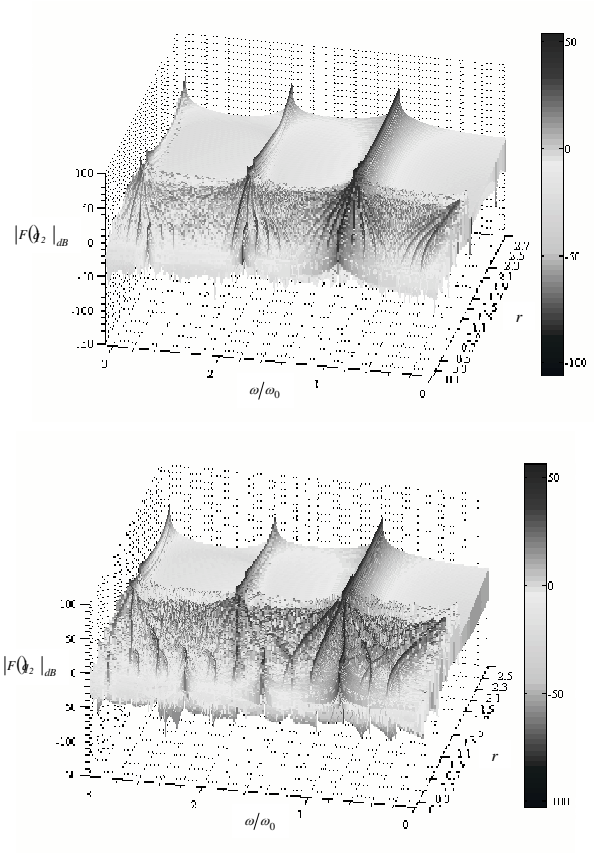

Figure 4: $|F\{\dot{q}_2(t)\}|$ of the $3R-$robot during 300 cycles, *vs* r and ω/ω_0, for $\rho = \{0.3,\ 0.5\}$, $\omega_0 = 7.0$ rad sec^{-1}.

3. Manipulators with vibrations

This section presents a fractional calculus perspective in the study of the robotic signals captured during an impact phase of the manipulator. In the experiment is used a steel rod flexible link. To test impacts, the link consists on a long, thin, round, flexible steel rod clamped to the end-effector of the manipulator. The robot motion is programmed in a way such that the rod moves against a rigid surface. During the motion of the manipulator the clamped rod is moved by the robot against a rigid surface. An impact occurs

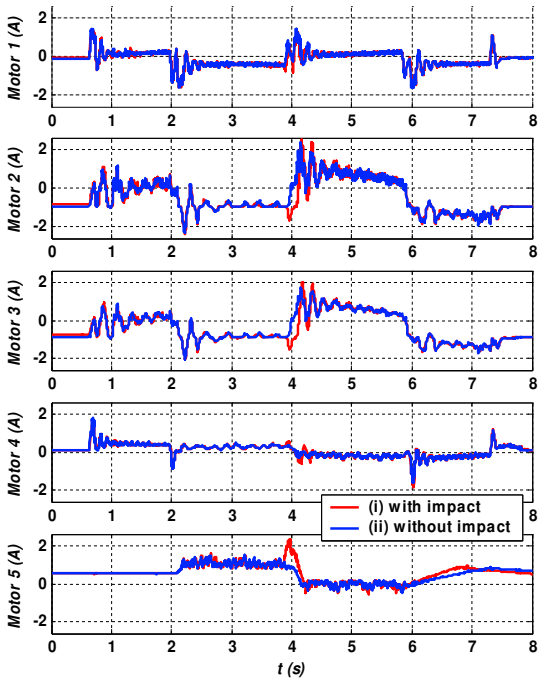

Figure 5: Electrical currents of robot axis motors.

and several signals are recorded with a sampling frequency of $f_s = 500$ Hz. In order to analyze the vibration and impact phenomena an acquisition system was developed [14]. The instrumentation system acquires signals from multiple sensors that capture the axis positions, mass accelerations, forces and moments and electrical currents in the motors. Afterwards, an analysis package, running off-line, reads the data recorded by the acquisition system and examines them. Due to space limitations only some of the signals are depicted. A typical time evolution of the electrical currents of robot axis motors is shown in **Fig. 5** corresponding to: (i) the impact of the rod on a rigid surface, and (ii) without impact [15]. In this example, the signals present clearly a strong variation at the instant of the impact that occurs, approximately, at $t = 4$ sec. In order to study the behavior of the signal Fourier transform, a trendline can be superimposed over the spectrum based

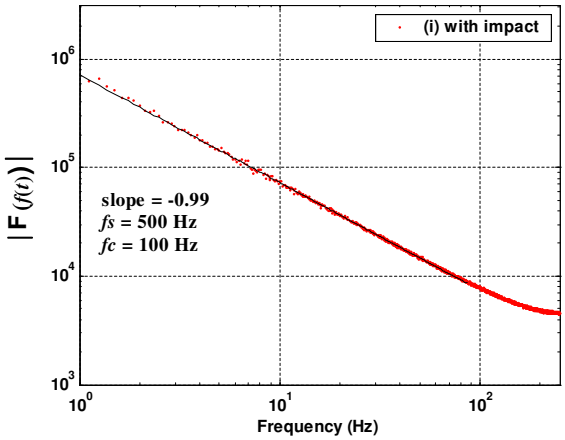

Figure 6: Spectrum of the axis 1 position.

on a power law approximation:

$$|F\{f(t)\}| \approx c\omega^m, \tag{9}$$

where $F\{\}$ is the Fourier operator, $c \in \Re^+$, ω is the frequency and $m \in \Re$ is the slope.

Fig. 6 shows the amplitude of the Fast Fourier Transform (FFT) of the axis 1 position signal. The trendline (9) leads to a slope $m = -0.99$ revealing, clearly, the integer order behavior. The others position signals were studied, revealing also an integer behavior, both under impact and no impact conditions. **Fig. 7** shows the amplitude of the FFT of the electrical current for the axis 3 motor. The spectrum was also approximated by trendlines in a frequency range larger than one decade. These trendlines (**Fig. 7**) have slopes of $m = -1.52$ and $m = -1.51$ under impact (i) and without impact (ii) conditions, respectively. The lines present a fractional order behavior in both cases. The others axis motor currents were studied, as well. Some of them, for a limited frequency range, present also fractional order behavior while others have a complicated spectrum difficult to approximate by one trendline. **Fig. 8** shows, as example, the spectrum of the F_z force. This spectrum is not so well defined in a large frequency range. All force/moments and acceleration spectra present identical behavior and, therefore, it is difficult to define accurately the behavior of the signals.

As shown in the examples, the Fourier spectrum of several signals, captured during an impact phase of the manipulator, presents a non integer be-

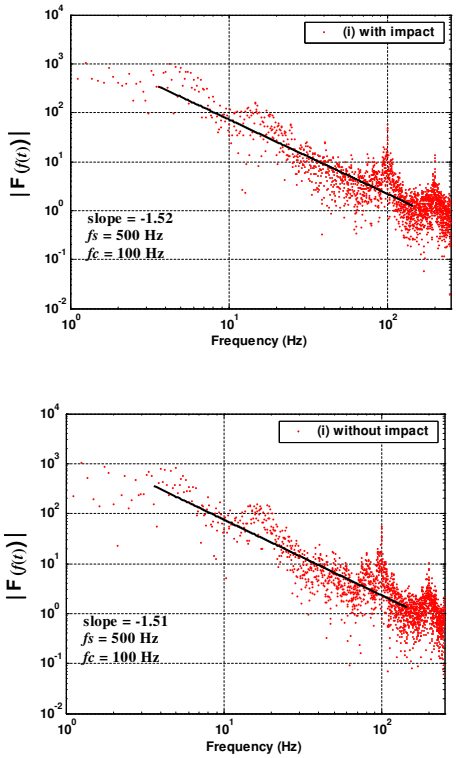

Figure 7: Spectrum of the axis 3 motor current.

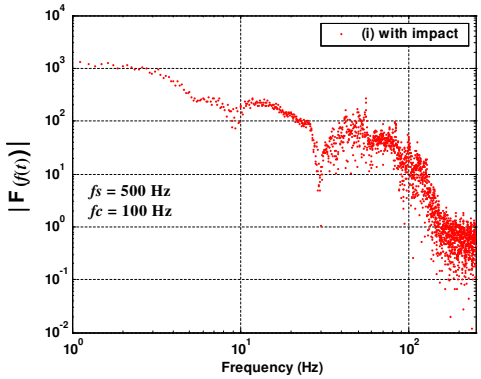

Figure 8: F_z force spectrum with impact.

havior. On the other hand, the feedback fractional order systems, due to the success in the synthesis of real noninteger differentiator and the emergence of fractional-order controllers, have been designed and applied to control a variety of dynamical processes [16]. Therefore the study presented here can assist in the design of the control system to be used in eliminating or reducing the effect of vibrations.

4. Manipulator position/force control

Raibert and Craig [19] introduced the concept of force control based on the hybrid algorithm and, since then, several researchers developed those ideas and proposed other schemes [20]. There are two basic methods for force control, namely the hybrid position/ force and the impedance schemes. The first method separates the task into two orthogonal sub-spaces corresponding to the force and the position controlled variables. Once established the subspace decomposition two independent controllers are designed. The second method [20] requires the definition of the arm mechanical impedance. The impedance accommodates the interaction forces that can be controlled to obtain an adequate response. The dynamical equation of a $n\ dof$ robot is:

$$\tau = \mathbf{C}(\mathbf{q}, \dot{\mathbf{q}}) + \mathbf{G}(\mathbf{q}) + \mathbf{H}(\mathbf{q})\ddot{\mathbf{q}} - \mathbf{J}^{\mathbf{T}}(\mathbf{q})\mathbf{F} \tag{10}$$

where τ is the $n \times 1$ vector of actuator torques, $\mathbf{q}$ is the $n \times 1$ vector of joint coordinates, $\mathbf{H(q)}$ is the $n \times n$ inertia matrix, $\mathbf{C}(\mathbf{q}, \dot{\mathbf{q}})$ is the $n \times 1$ vector of centrifugal / Coriolis terms and $\mathbf{G(q)}$ is the $n \times 1$ vector of gravitational effects. The matrix $\mathbf{J}^T\mathbf{(q)}$ is the transpose of the Jacobian and $\mathbf{F}$ is the force that the load exerts in the robot gripper. For a $2R-$robot the dynamics yields:

$$\mathbf{C}\left(\mathbf{q}, \dot{\mathbf{q}}\right) = \begin{bmatrix} -m_2 r_1 r_2 S_2 \dot{q}_2^2 - 2m_2 r_1 r_2 S_2 \dot{q}_1 \dot{q}_2 \\ m_2 r_1 r_2 S_2 \dot{q}_1^2 \end{bmatrix} \tag{11}$$

$$\mathbf{G}\left(\mathbf{q}\right) = \begin{bmatrix} g\left(m_1 r_1 C_1 + m_2 r_1 C_1 + m_2 r_2 C_{12}\right) \\ g m_2 r_2 C_{12} \end{bmatrix} \tag{12}$$

$$\mathbf{J^T}\left(\mathbf{q}\right) = \begin{bmatrix} -r_1 S_1 - r_2 S_{12} & r_1 C_{11} + r_2 C_{12} \\ -r_2 S_{12} & r_2 C_{12} \end{bmatrix} \tag{13}$$

$$\mathbf{H}\left(\mathbf{q}\right) = \begin{bmatrix} (m_1 + m_2) r_1^2 - m_2 r_2^2 & m_2 r_2^2 + m_2 r_1 r_2 C_2 \\ +2m_2 r_1 r_2 C_2 + J_{1m} + J_{1g} & \\ -m_2 r_2^2 + m_2 r_1 r_2 C_2 & m_2 r_2^2 + J_{2m} + J_{2g} \end{bmatrix} \tag{14}$$

where $C_{ij} = \cos(q_i + q_j)$ and $S_{ij} = \sin(q_i + q_j)$.

The numerical values adopted for the $2R-$robot [21] are $m_1 = 0.5$ kg, $m_2 = 6.25$ kg, $r_1 = 1.0$ m, $r_2 = 0.8$ m, $J_{1m} = J_{2m} = 1.0$ kgm^2 and $J_{1g} = J_{2g} = 4.0\ kgm^2$. The constraint plane is determined by the angle θ (**Fig. 9**) and the contact displacement x_c of the robot gripper with the constraint surface is modeled through a linear system with a mass M, a damping B and a stiffness K with dynamics:

$$F_c = M\ddot{x_c} + B\dot{x_c} + Kx_c \tag{15}$$

In order to study the dynamics and control of one robot we adopt the position/force hybrid control with the implementation of the integer order and fractional-order algorithms [13], [16], [17], [18], [22], [23]. The system performance and robustness is analyzed in the time domain. The effect of dynamic backlash and flexibility is also investigated.

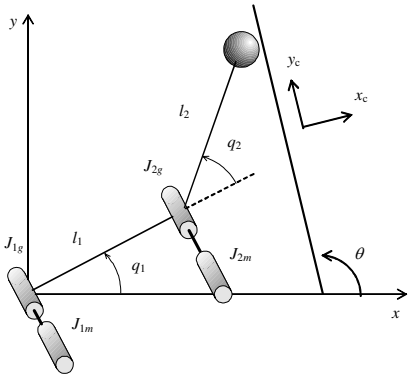

Figure 9: The $2R-$robot and the constraint surface.

The structure of the position/force hybrid control algorithm is depicted in **Fig. 10**. The diagonal $n \times n$ selection matrix $\mathbf{S}$ has elements equal to one (zero) in the position (force) controlled directions and $\mathbf{I}$ is the $n \times n$ identity matrix. In this paper the y_c, (x_c) cartesian coordinate is position (force) controlled, yielding:

$$\mathbf{S} = \begin{bmatrix} 1 & 0 \\ 0 & 1 \end{bmatrix}, \quad \mathbf{J}_c(\mathbf{q}) = \begin{bmatrix} -l_1 C_{\theta 11} - l_2 C_{\theta 12} & -l_2 C_{\theta 12} \\ l_1 S_{\theta 11} + l_2 S_{\theta 12} & +l_2 S_{\theta 12} \end{bmatrix} \tag{16}$$

We now analyze the system performance both for ideal transmissions and robots with dynamic phenomena at the joints, such as backlash and flexibility. Moreover, we compare the response of FO and the PD: $C_P(s) = K_p$

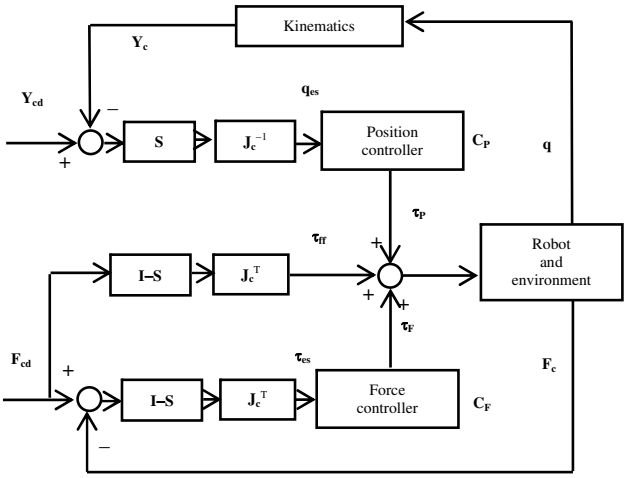

Figure 10: The position/force hybrid controller.

$+ K_d\, s$ and PI: $C_F(s) = K_p + K_i\, s^{-1}$ controllers, in the position and force loops. Both algorithms were tuned by trial and error having in mind getting a similar performance in the two cases. The resulting parameters were FO: $\{K_P,\ \alpha_P\} \equiv \{10^5,\ 1/2\}$, $\{K_F,\ \alpha_F\} \equiv \{10^3,\ 1/5\}$ and $PD-PI$: $\{K_p,K_d\} \equiv \{10^4,\ 10^3\}$, $\{K_p,\ K_i\} \equiv \{10^3,\ 10^2\}$ for the position and force loops, respectively. Moreover, it is adopted the operating point $\{x,\ y\} \equiv \{1,\ 1\}$, a constraint surface with parameters $\{\theta,\ M,\ B,\ K\} \equiv \{\pi/2, 10^3, 1.0, 10^2\}$ and a controller sampling frequency $f_c = 1$ kHz. In order to study the system dynamics we apply, separately, rectangular pulses, at the position and force references, that is, we perturb the references with $\{y_{cd},\ F_{cd}\} = \{10^{-1},\ 0\}$ and $\{y_{cd},\ F_{cd}\} = \{0,\ 10^{-1}\}$. **Fig. 11** depicts the time response of the $2R-$robot under the action of the FO and the $PD-PI$ controllers for ideal transmissions at the joints.

In a second phase (**Fig. 12**) we analyze the response of robots with dynamic backlash at the joints. For the i^{th} joint ($i = 1,\ 2$), with gear clearance h_i, the backlash reveals impact phenomena between the inertias, which obey the principle of conservation of momentum and the Newton law:

$$\dot{q}_i' = \frac{\dot{q}_i\,(J_{ii} - \varepsilon J_{im}) + \dot{q}_{im} J_{im}\,(1+\varepsilon)}{J_{ii} + J_{im}}\,, \tag{17}$$

$$\dot{q}_{im}' = \frac{\dot{q}_i J_i\,(1+\varepsilon) + \dot{q}_{im}\,(J_{im} - \varepsilon J_{ii})}{J_{ii} + J_{im}}\,, \tag{18}$$

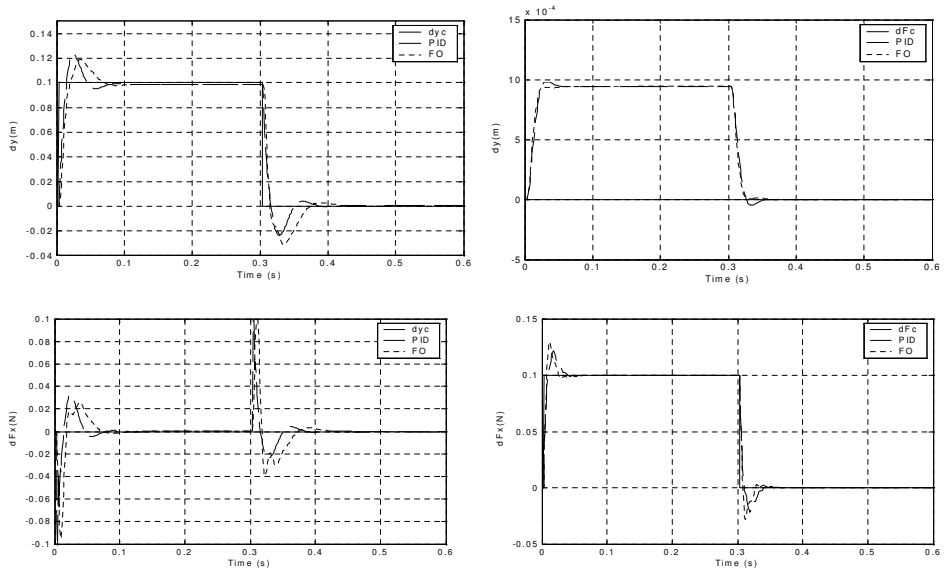

Figure 11: Time response for the $2R-$robot with ideal transmission at the joints under the action of the FO and $PD-PI$ controllers for pulses perturbations $\delta y_{cd} = 10^{-1}$ m and $\delta F y_{cd} = 10^{-1}$ Nm at the robot position and force references, respectively.

where $0 \leq \varepsilon \leq 1$ is a constant that defines the type of impact ($\varepsilon = 0$ inelastic impact, $\varepsilon = 1$ elastic impact) and $\dot{q}_i$ and $\dot{q}_{im}$ ($\dot{q}'_i$ and $\dot{q}'_{im}$) are the velocities of the i^{th} joint and motor before (after) the collision, respectively. The parameter J_{ii} (J_{im}) stands for the link (motor) inertias of joint i. In the simulations is adopted $h_i = 1.8\ 10^{-4}$ rad and $\varepsilon_i = 0.8$.

In a third phase (**Fig. 13**) it is studied the case of compliant joints, where the dynamic model corresponds to (10) augmented by the equations:

$$\mathbf{T} = \mathbf{J}_m \ddot{\mathbf{q}}_m + \mathbf{B}_m \dot{\mathbf{q}}_m + \mathbf{K}_m(\mathbf{q}_m\text{-}\mathbf{q}), \tag{19}$$

$$\mathbf{K}_m(\mathbf{q}_m\text{-}\mathbf{q}) = \mathbf{J}(\mathbf{q})\ddot{\mathbf{q}} + \mathbf{C}(\mathbf{q}, \dot{\mathbf{q}}) + \mathbf{G}(\mathbf{q}), \tag{20}$$

where $\mathbf{J}_m$, $\mathbf{B}_m$ and $\mathbf{K}_m$ are the $n \times n$ diagonal matrices of the motor and transmission inertias, damping and stiffness, respectively. In the simulations we adopt $\mathbf{K}_{mi} = 2.0\ 10^6$ Nm rad^{-1} and $\mathbf{B}_{mi} = 10^4$ Nms rad^{-1} (i = 1,2).

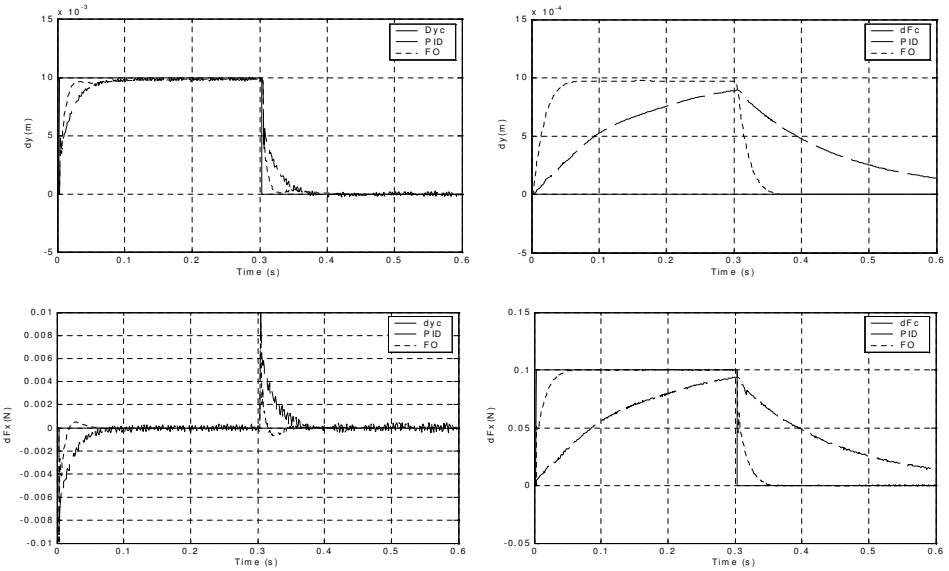

Figure 12: Time response for $2R-$robot with dynamic backlash at the joints under the action of the FO and $PD-PI$ controllers for pulses perturbations $\delta y_{cd} = 10^{-1}$ m and $\delta F y_{cd} = 10^{-1}$ Nm at the robot position and force references, respectively.

Table 1: Time response for a pulse δy_{cd} at the robot reference.

No	$C(s)$	$PO\%$	e_{ss}[m]	T_p[s]	T_s[s]
$ideal$	$PD-PI$	23.48	99.0 10^{-3}	0.122 10^{-2}	13.0 10^{-2}
	FO	18.98	79 10^{-3}	3.36 10^{-2}	18.0 10^{-2}
$backlash$	$PD-PI$	0.37	2.1 10^{-3}	38.0 10^{-2}	8.0 10^{-2}
	FO	0.36	1.4 10^{-4}	3.0 10^{-2}	11.8 10^{-2}
$flexible$	$PD-PI$	2.28	3.9 10^{-3}	40.3 10^{-2}	15.0 10^{-1}
	FO	1.8	1.4 10^{-3}	30.2 10^{-2}	30.4 10^{-1}

Table 2: Time response for a pulse δFy_{cd} at the robot reference.

No	$C(s)$	$PO\%$	e_{ss}[m]	T_p[s]	T_s[s]
ideal	$PD-PI$	22.0	1.3 10^{-3}	8.0 10^{-3}	9.1 10^{-2}
	FO	29.50	1.3 10^{-3}	8.9 10^{-3}	9.3 10^{-2}
backlash	$PD-PI$	5.98	9.9 10^{-3}	4.0 10^{-1}	4.0 10^{-2}
	FO	8.6	9.9 10^{-3}	7.9 10^{-2}	4.0 10^{-2}
flexible	$PD-PI$	3.2	9.9 10^{-2}	6.0 10^{-2}	6.0 10^{-1}
	FO	1.8	9.9 10^{-3}	4.0 10^{-1}	4.5 10^{-1}

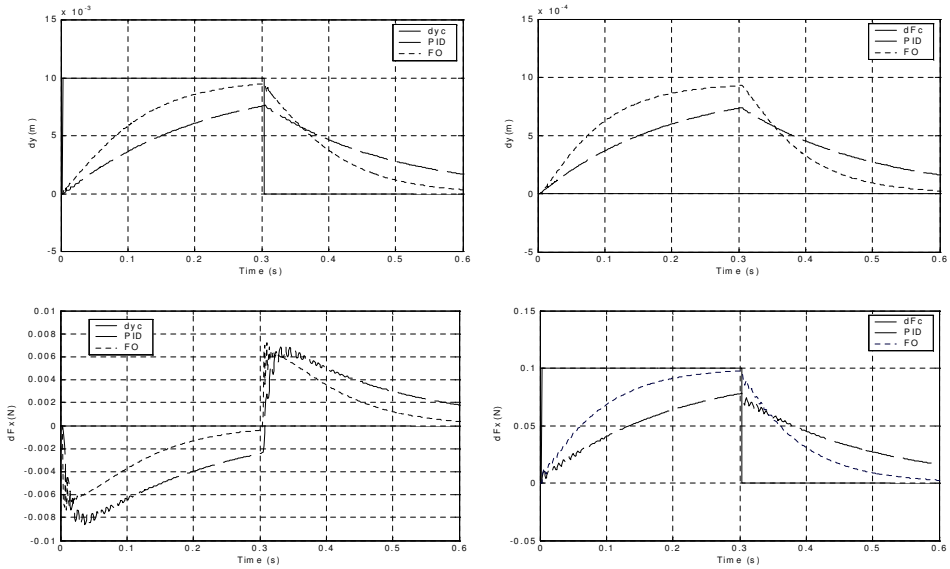

Figure 13: Time response for $2R-$robot with flexibility at the joints under the action of the FO and $PD-PI$ controllers for pulses perturbations $\delta y_{cd} = 10^{-1}$ m and $\delta Fy_{cd} = 10^{-1}$ Nm at the robot position and force references, respectively.

The time responses (**Tables 1 and 2**), namely the percent overshoot $PO\%$, the steady-state error e_{ss}, the peak time T_p and the settling time T_s, reveal that, although tuned for similar performances in the first case, the FO is superior to the $PD-PI$ in the cases with dynamical phenomena at the robot joints.

It is clear that the FO demonstrates better performance for joints having nonlinearities.

5. Control of two cooperating manipulators

Two robots carrying a common object are a logical alternative for the case in which a single robot is not able to handle the load. The choice of a robotic mechanism depends on the task or the type of work to be performed and, consequently, is determined by the position of the robots and by their dimensions and structure. In general, the selection is done through experience and intuition; nevertheless, it is important to measure the manipulation capability of the robotic system [24] that can be useful in the robot operation. In this perspective it was proposed the concept of kinematic manipulability [25] and its generalization by including the dynamics [26] or, alters natively, the statistical evaluation of manipulation. Other related aspects such as the coordination of two robots handling objects, collision avoidance and free path planning have been also investigated [27]. With two cooperative robots the resulting interaction forces have to be accommodated and consequently, in addition to position feedback, force control is also required to accomplish adequate performances [28], [29]. We consider two $2R$ cooperating manipulators with identical dimensions. The contact of the robot gripper with the load is modeled through a linear system with a mass M, a damping B and a stiffness K (**Fig. 14**).

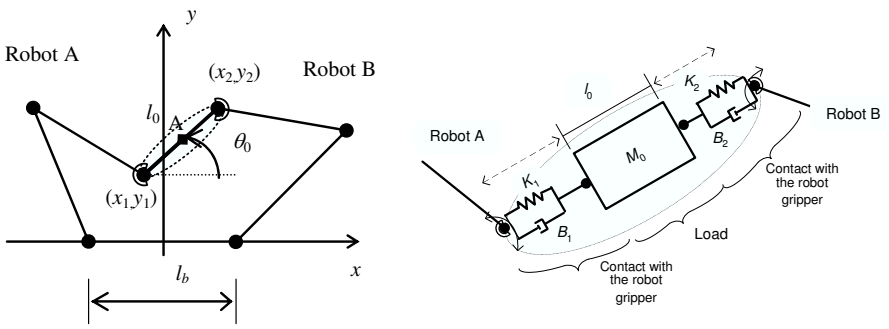

Figure 14: The $2R$ dual arm robot and the contact between the robot gripper and the object.

The controller architecture (**Fig. 15**) is inspired on the impedance and compliance schemes. Therefore, we establish a cascade of force and position algorithms as internal an external feedback loops, respectively, where x_d and F_d are the payload desired position coordinates and contact forces.

We analyze the system performance both for robots ideal transmissions and robots with dynamic phenomena at the joints, such as backlash and flexibility. Moreover, we compare the response of FO and classical algorithms

namely PD: $C_P(s) = K_p\,(1+T_d s)$ and PI: $C_F(s) = K_F\,[1+(T_i s)^{-1}]$, in the position and force loops, respectively. Both algorithms were tuned by trial and error having in mind getting a similar performance in the two cases. The resulting parameters were FO: $\{K_P, \alpha_P\} \equiv \{10^4, 1/2\}$, $\{K_F, \alpha_F\} \equiv \{2, 1/5\}$ and $PD-PI$: $\{K_p, K_d\} \equiv \{10^4, 10^2\}$, $\{K_p, K_i\} \equiv \{10, 10^4\}$ for the position and force loops, respectively. Moreover, it is adopted the operating point, the center of the object A $\equiv \{x, y\} \equiv \{0, 1\}$ and a object surface with parameters $\{\theta, M, B_j, K_j\} \equiv \{0, 10.0, 1.0, 10^3\}$. In order to study the system dynamics we apply, separately, small amplitude rectangular pulses, at the position and force references. Therefore, we perturb the references with $x_d = 10^{-3}$, $y_d = 10^{-3}$, $F_{xd} = 1.0$, $F_{yd} = 1.0$ and we analyze the system performance in the time domain. To evaluate the performance of the proposed algorithms we compare the response for robots with dynamical phenomena at the joints. In all experiments the controller sampling frequency is $f_c = 10$ kHz for the operating point A of the object and a contact force of each gripper of $\{F_{xj}, F_{yj}\} \equiv \{0.5, 5\}$ Nm for the jth ($j = 1, 2$) robot. **Fig. 16** depicts the time response of the robot A, under the action of the FO and the $PD-PI$ algorithms, for robots with ideal transmissions at the joints.

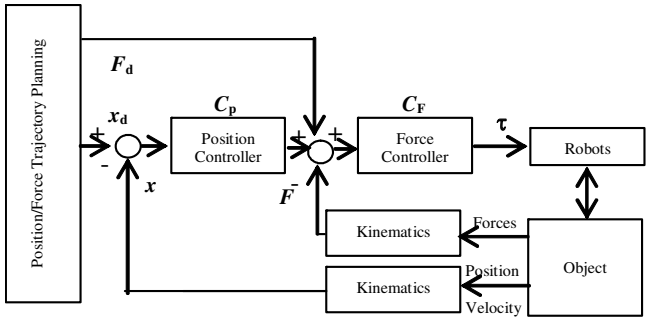

Figure 15: The position/force cascade controller.

In **Figs. 17 and 18** we analyze the response of robots with dynamic backlash and dynamic flexibility at the joints.

The time responses (**Tables 3-6**), namely the percent overshoot $PO\%$, the steady-state error e_{ss}, the peak time T_p and the settling time T_s reveal that, although tuned for almost similar performances in the first case, the FO is superior to the $PD-PI$ algorithms in the cases of robots with joint dynamic phenomena.

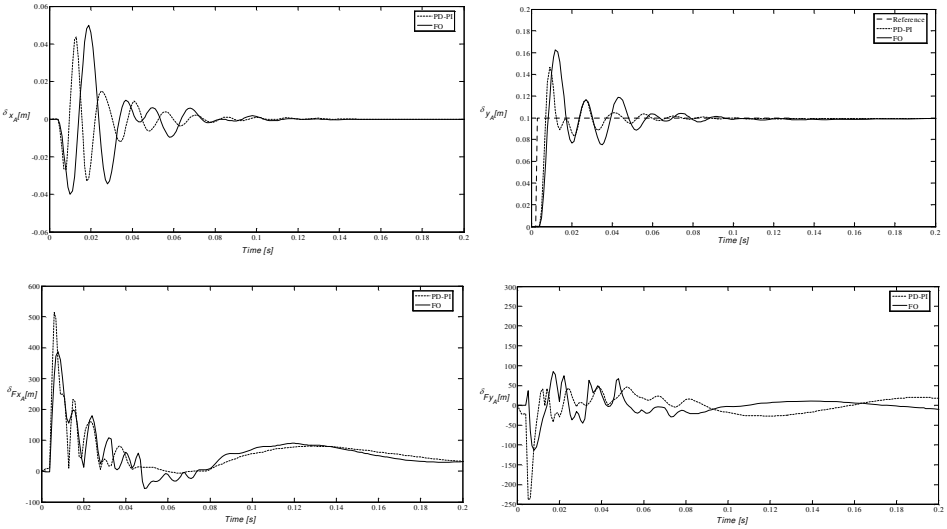

Figure 16: The time response of robots with ideal joints under the action of the FO and the $PD-PI$ algorithms for a pulse perturbation at the robot A position reference $\delta y_d = 10^{-3}$ m and a payload $M = 1.0$ kg, $B_i = 1.0$ Ns/m and $K_i = 10^3$ N/m.

Table 3: Time response for a pulse δy_d at the robot A reference.

No	$C(s)$	$PO\%$	e_{ss}[m]	T_p[s]	T_s[s]
$ideal$	$PD-PI$	39.0	5.0 10^{-3}	1.1 10^{-2}	25.0 10^{-2}
	FO	43.0	0.9 10^{-3}	1.6 10^{-2}	15.0 10^{-2}
$backlash$	$PD-PI$	0.2	2.7 10^{-2}	37.0 10^{-2}	5.0 10^{-1}
	FO	0.2	3.5 10^{-3}	4.0 10^{-2}	4.0 10^{-2}
$flexible$	$PD-PI$	0.3	64.0 10^{-2}	38.0 10^{-2}	45.0 10^{-2}
	FO	0.3	50.0 10^{-3}	25.0 10^{-2}	19.0 10^{-2}

Table 4: Time response for a pulse δFy_d at the robot A reference.

No	$C(s)$	$PO\%$	e_{ss}[m]	T_p[s]	T_s[s]
$ideal$	$PD-PI$	400.0	9.8 10^{-1}	1.1 10^{-2}	2.0 10^{-1}
	FO	115.0	77.0 10^{-3}	25.0 10^{-2}	5.0 10^{-1}
$backlash$	$PD-PI$	400.0	9.8 10^{-1}	1.1 10^{-2}	2.0 10^{-1}
	FO	100.0	77.0 10^{-3}	20.0 10^{-2}	4.0 10^{-1}
$flexible$	$PD-PI$	100.0	9.8 10^{-1}	1.1 10^{-2}	1.0 10^{-1}
	FO	100.0	77.0 10^{-3}	20.0 10^{-2}	4.0 10^{-1}

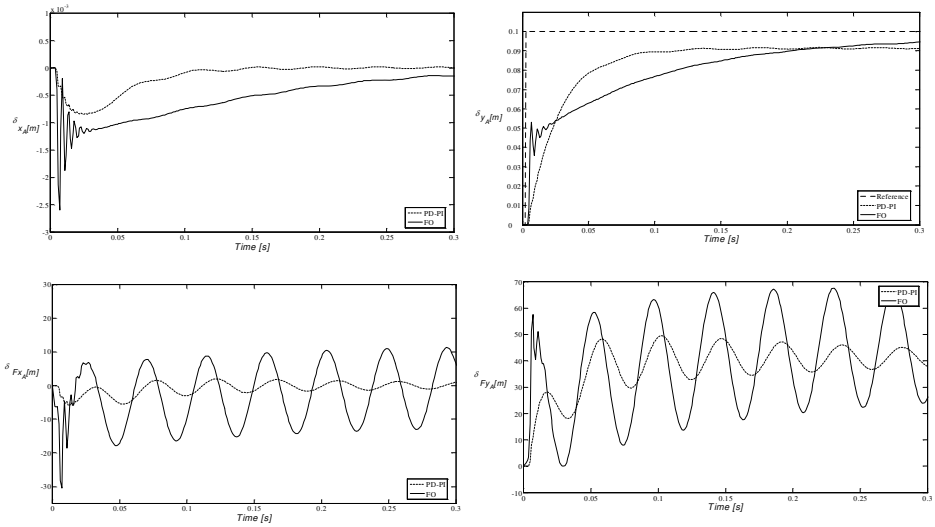

Figure 17: The time response of robots with joints having backlash under the action of the FO and the $PD-PI$ algorithms for a pulse perturbation at the robot A position reference $\delta y_d = 10^{-3}$ m and a payload $M = 1$ kg, $B_i = 1$ Ns/m and $K_i = 10^3$ N/m.

Table 5: Time response for a pulse δy_d at the robot A reference.

No	$C(s)$	$PO\%$	e_{ss}[m]	T_p[s]	T_s[s]
ideal	$PD-PI$	39.0	5.0 10^{-3}	1.1 10^{-2}	25.0 10^{-2}
	FO	43.0	0.9 10^{-3}	1.6 10^{-2}	15.0 10^{-2}
backlash	$PD-PI$	0.2	2.7 10^{-2}	37.0 10^{-2}	5.0 10^{-1}
	FO	0.2	3.5 10^{-3}	4.0 10^{-2}	4.0 10^{-2}
flexible	$PD-PI$	0.3	64.0 10^{-2}	38.0 10^{-2}	45.0 10^{-2}
	FO	0.3	50.0 10^{-3}	25.0 10^{-2}	19.0 10^{-2}

Table 6: Time response for a pulse δFy_d at the robot A reference.

No	$C(s)$	$PO\%$	e_{ss}[m]	T_p[s]	T_s[s]
ideal	$PD-PI$	400.0	9.8 10^{-1}	1.1 10^{-2}	2.0 10^{-1}
	FO	115.0	77.0 10^{-3}	25.0 10^{-2}	5.0 10^{-1}
backlash	$PD-PI$	400.0	9.8 10^{-1}	1.1 10^{-2}	2.0 10^{-1}
	FO	100.0	77.0 10^{-3}	20.0 10^{-2}	4.0 10^{-1}
flexible	$PD-PI$	100.0	9.8 10^{-1}	1.1 10^{-2}	1.0 10^{-1}
	FO	100.0	77.0 10^{-3}	20.0 10^{-2}	4.0 10^{-1}

4. Conclusions

The recent progress in the area of nonlinear dynamics and chaos promises a large area of application of the theory of FC. In the area of dynamical system modeling and control preliminary work has been proposed but many areas are still to be explored. In this paper several aspects of mechanical manipulator analysis and control were addressed, namely, path planning of redundant manipulators, vibration analysis in mechanical systems, and position/force control both on single and dual robotic arms involving several types on nonlinear dynamical phenomena. The results demonstrate that FC constitutes a mathematical tool to be considered for the development of robotic systems with superior performances.

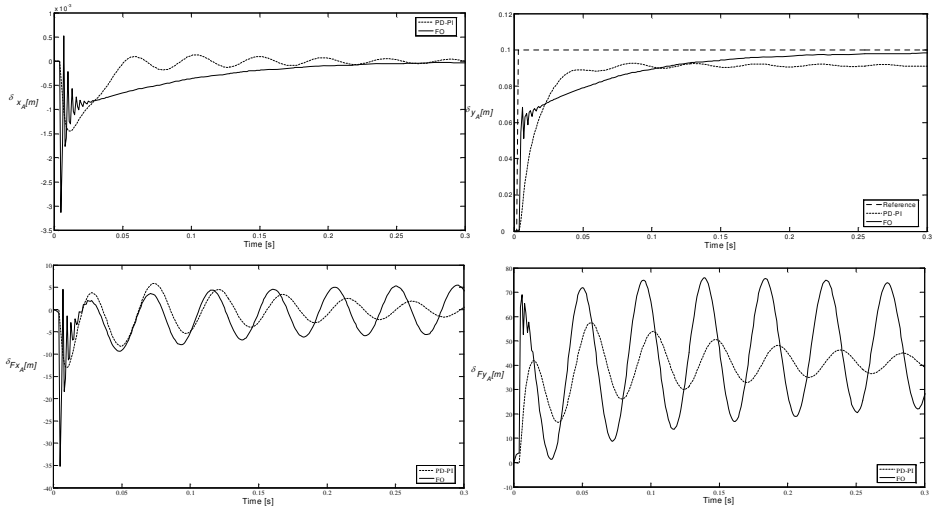

Figure 18: Time response of robots with joints having flexibility under the action of the FO and the $PD-PI$ algorithms, for a pulse perturbation at the robot A position reference $\delta y_d = 10^{-3}$ m and a payload $M = 1$ kg, $B_i = 1$ Ns/m and $K_i = 10^3$ N/m.

References

[1] E. S. Conkur and R. Buckingham, Clarifying the definition of redundancy as used in robotics. *Robotica* **15**, No 5 (1997), 583-586.

[2] S. Chiaverini, Singularity-robust task-priority redundancy resolution for real time kinematic control of robot manipulators. *IEEE Trans. Robotics Automation* **13**, No 3 (1997), 398-410.

[3] C.A Klein and C. C Huang, Review of pseudoinverse control for use with kinematically redundant manipulators. *IEEE Trans. Syst. Man, Cyber.* **SMC-13**, No 2 (1983), 245-250.

[4] T. Yoshikawa, *Foundation of Robotics: Analysis and Control.* MIT Press (1988).

[5] John Bay, Geometry and prediction of drift-free trajectories for redundant machines under pseudoinverse control. *Journal of Intelligent and Robotic Systems* **11**, No 1 (1992), 41-52.

[6] Y. Nakamura, *Advanced Robotics: Redundancy and Optimization.* Addison-Wesley (1991).

[7] Keith L. Doty, C. Melchiorri and C. Bonivento, A theory of generalized inverses applied to robotics. *Journal of Intelligent and Robotic Systems* **12**, No 1 (1993), 1-19.

[8] Bruno Siciliano, Kinematic control of redundant robot manipulators: a tutorial. *Journal of Intelligent and Robotic Systems* **3**, No 3 (1990), 201-212.

[9] Sanjeev Seereeram and John T. Wen, A global approach to path planning for redundant manipulators. *IEEE Trans. Robotics Automation* **11**, No 1 (1995), 152-160.

[10] Fernando Duarte and J. Tenreiro Machado, Chaotic phenomena and fractional-order dynamics in the trajectory control of redundant manipulators. *Nonlinear Dynamics (Kluwer)* **29**, Nos 1-4 (2002), 315-342.

[11] J. A. Tenreiro Machado, Analysis and design of fractional-order digital control systems. *Journal Systems Analysis-Modelling-Simulation* **27** (1997), 107-122.

[12] J. A. Tenreiro Machado, Discrete-time fractional-order controllers. *Fractional Calculus & Applied Analysis* **4**, No 1 (2001), 47-66.

[13] Maria Graça Marcos, Fernando Duarte and J. A. Tenreiro Machado, Complex dynamics in the trajectory control of redundant manipulators. *Nonlinear Science and Complexity (World Scientific)*, **1** (2007), 134-143.

[14] Miguel F. M. Lima, J.A. Tenreiro Machado and Manuel Crisóstomo, Experimental set-up for vibration and impact analysis in robotics. *WSEAS Trans. on Systems, Issue 5* **4**, No 2 (2005), 569-576.

[15] Miguel Lima, J. A. Tenreiro Machado and Manuel Crisóstomo, Fractional order Fourier spectra in robotic manipulators with vibrations. In: *Second IFAC Workshop on Fractional Differentiation and its Applications*, Porto, Portugal (2006).

[16] Alain Oustaloup, *La commande CRONE: commande robuste d'ordre non entier*. Editions Hermès, Paris (1991).

[17] Alain Oustaloup, *La dérivation non entière: théorie, synthèse et applications*. Editions Hermès, Paris (1995).

[18] R. S. Barbosa, J. A. Tenreiro Machado and I. M. Ferreira, Tuning of PID controllers based on bode's ideal transfer function. *Nonlinear Dynamics (Kluwer)* **38**, Nos 1-4 (2004), 305-321.

[19] M. H. Raibert and J. J. Craig, Hybrid position/force control of manipulators. *ASME J. of Dynamic Systems, Measurement and Control* **103**, No 2 (1981), 126-133.

[20] N. Hogan, Impedance control: An approach to manipulation, Parts: I-Theory, II-Implementation, III-Applications. *ASME J. of Dynamic Systems, Measurement and Control* **107**, No 1 (1985), 1-24.

[21] O. Khatib, A unified approach for motion and force control of robot manipulators: the operational space formulation. *IEEE Journal of Robotics and Automation* **3**, No 1 (1987), 43-53.

[22] B. Siciliano and L. Villani, A force/position regulator for robot manipulators without velocity measurements. *IEEE Int. Conf. on Robotics and Automation* **3** (1996), 2567-2572.

[23] N. M. Fonseca Ferreira and J. A. Tenreiro Machado, fractional-order hybrid control of robotic manipulator. In: *10th IEEE Int. Conf. on Advanced Robotics, Coimbra, Portugal* **1** (2003), 221-229.

[24] Y. C. Tsai and A.H Soni, Accessible region and synthesis of robot arms. *ASME J. Mech. Design* **103** (1981), 803-811.

[25] T. Yoshikawa, Manipulability of robotic mechanisms. *Int. J. Robotics Research* **4**, No 2 (1985), 3-9.

[26] H. Asada, A geometrical representation of manipulator dynamics and its application to arm design. *ASME J. of Dynamic Systems, Measurement and Control* **105** (1983), 131-142.

[27] Y. Nakamura, K. Nagai and T. Yoshikawa, Dynamics and stability in coordination of multiple robotic mechanisms. *International Journal of*

Robotics Research **8** (1989), 44-61.

[28] N. M. Fonseca Ferreira and J. A. Tenreiro Machado, Manipulability analysis of two-arm robotic systems. In: *4th IEEE International Conference on Intelligent Engineering Systems* (2000), 101-109.

[29] N. M. Fonseca Ferreira, J. A. Tenreiro Machado and J. Boaventura Cunha, Fractional - order position/force robot control. In: *2nd IEEE Int. Conference on Computational Cybernetics*, Vienna, Austria (2004), 126-133.

Received: December 20, 2007

[1] *Institute of Engineering of Coimbra*
Dept. of Electrical Engineering
Rua Pedro Nunes, 3031-601 Coimbra, PORTUGAL
e-mail: nunomig@isec.pt

[2] *School of Technology of Viseu*
Dept. of Mathematics
3504-510 Viseu, PORTUGAL
e-mail: fduarte@mat.estv.ipv.pt

[3] *School of Technology of Viseu*
Dept. of Electrical Engineering
3504-510 Viseu, PORTUGAL
e-mail: lima@mail.estv.ipv.pt

[4] *Institute of Engineering of Porto*
Dept. of Mathematics
Rua Dr António Bernardino de Almeida
4200-072 Porto, PORTUGAL
e-mail: mgm@isep.ipp.pt

[5] *Institute of Engineering of Porto*
Dept. of Electrical Engineering
Rua Dr António Bernardino de Almeida
4200-072 Porto, PORTUGAL
e-mail: jtm@isep.ipp.pt